Available online at www.sciencedirect.com

ScienceDirect

Procedia Engineering 102 (2015) 1793 – 1802

Procedia Engineering

www.elsevier.com/locate/procedia

The 7th World Congress on Particle Technology (WCPT7)

Discrete element modeling of rock materials with dilated polyhedral elements

Shunying Ji[a,*], Shanshan Sun[a], Ying Yan[b]

[a]*State Key Laboratory of Structural Analysis for Industrial Equipment, Dalian University of Technology, Dalian 116023 China*
[b]*School of Civil and Safety Engineering, Dalian Jiaotong University, Dalian, China*

Abstract

Considering the irregular shapes of rock particles, a three dimensional dilated polyhedral element is generated with the Minkowski Sums operator. This dilated element can also be constructed with a basic sphere and real polyhedron based on the theory of Minkowski Sums. The element generation, contact resolution and detection are introduced in this paper. All inter-element contacts are grouped as three categories: edge-edge, vertex-surface, and surface - surface. This dilated polyhedral element is applied to simulate the dynamic behaviours of rock rubbles of railway ballast. The settlement and the bulk stiffness of ballast are analyzed under cyclic loading. The ballast particles are mixed randomly with initial dense packing. The results showed that permanent deformation increased with the loading frequency and number of loading cycle. The influence of inter-element friction is tested in the DEM simulations. In the next study of dilated polyhedral elements, the parallel algorithm of GPU technique will be developed to improve the computational efficiency.

Selection and peer-review under responsibility of Chinese Society of Particuology, Institute of Process Engineering, Chinese Academy of Sciences (CAS)

Keywords: discrete element method; dilated polyhedral element; Minkowski sums; railway ballast; cyclic loading.

* Corresponding author. Tel.: +86-411-8470-7212; fax: +86-411-8470-7212.
E-mail address: jisy@dlut.edu.cn

Selection and peer-review under responsibility of Chinese Society of Particuology, Institute of Process Engineering, Chinese Academy of Sciences (CAS)
doi:10.1016/j.proeng.2015.01.316

1. INTRODUCTION

Under the action of cyclic loadings, the elastic property of railway ballast track will be reduced in long period operation accompanying the increase of accumulated settlement of ballast bed. The investigations on dynamic behaviors of ballast track under cyclic loadings can improve the ballast bed design and performance. Recent years, as a successful method for granular materials modeling, the discrete element method (DEM) has been applied widely to simulate the dynamic behaviors of ballast materials [1-4].

In the DEM simulation of ballast materials, the bonded clumps and overlapped particles were generated to model the irregular ballast particles [5-7]. In both of the bonded and the overlapped methods, one ballast particle is constructed with couple, tens, even hundreds spheres. It needs a huge number of sphere elements in the DEM simulation of ballast behaviors. Recently, a dilated polyhedron model was developed to model the irregular rock rubbles. The dilated polyhedron element can be generated with the theory of Minkowski sums [8-10]. In this method, a basic sphere with a defined radius is put on the surface of a polyhedron is to generate a smoothed polyhedron. Therefore, this dilated polyhedron is also called as spheropolygon [9,11]. The sharpness of polyhedron element can be defined with the basic sphere radius. With this polyhedron model, the element contact detection and contact force can be performed succinctly. Thus, the dilated polyhedron approach, as a special discrete element method, has a high computational efficiency for irregular particles. The polyhedron elements can be generated using Voronoi diagram with defined size and shapes randomly. With the combination of Voronoi diagram and Minkowski sums, the dilated polyhedrons are created simply [11].

In this study, we will construct the ballast particles with dilated polyhedrons based on Minkowski sums. The contact detection and contact force model of dilated polyhedrons are presented. The effective stiffness and degradation of ballast materials are simulated under cyclic loadings with different frequencies.

2. DILATED POLYHEDRON MODEL OF BALLAST PARTICLES

2.1 Construction of dilated polyhedrons

To construct a dilated polyhedron element, a basic polyhedron is defined firstly with vertexes, edges and planes. The polyhedron surface is generated with a series triangle planes. Then a dilating sphere with radius r is also adopted here. Based on the theory of Minkowski sums, the dilated polyhedron is generated by sweeping one set around the other, with out changing their relative orientation [11]. We can also image that the center of dilated sphere are put on the surface of the original polyhedron surface, including any vertex, edge and plane. With this approach, the dilated polyhedron element has smooth surfaces, round edges and round vertexes. Thus, the original vertex and edge of polyhedron become the sphere and cylinder of the dilated polyhedron, respectively. The planes still keep as planes.

A dilated polyhedron is generated as shown in Figure 1(a). The sharpness of the dilated polyhedron can be dominated with the dilating sphere radius. In Figure 1(b) and (c), the two dilated polyhedron elements are constructed with same basic polyhedron but different sphere radiuses of 0.01m and 0.2m, respectively. The more small the sphere radius, the more sharp the dilated polyhedron element performs. When the sphere radius approaches zero, the dilated polyhedron returns to the basic polyhedron. With this Minkowski sum method, various dilated polyhedron elements are generated, as shown in Figure 2. Here, we try to generate the ballast particles with the less vertexes and planes to improve the computational efficiency.

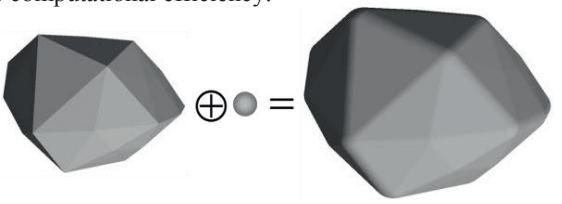

(a). Construction of a dilated polyhedron with a basic polyhedron and a dilating sphere based on Minkowski sums

(b). sphere radius r =0.01m (c). sphere radius r =0.2m

Figure 1. Generation of dilated polyhedron with Minkowski sum

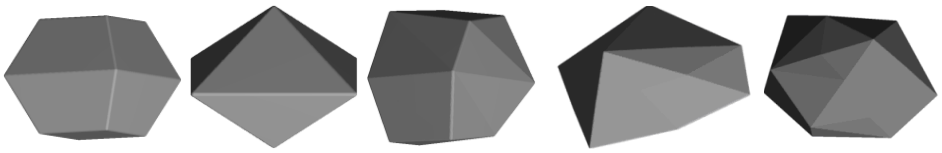

Figure 2. Some dilated polyhedrons constructed for ballast particles

2.2 Neighbor searching and contact detection of dilated polyhedron elements

Before the contact detections of dilated polyhedron elements, the neighbor list of each element should be determined firstly with their location and effective size. The elements are sorted with their mass center locations into a three dimensional Cartesian grids. The grid length is a little larger than the maximum size of elements. The potential contact neighbors of the concerned element will be listed from its surrounding grids. To determine the neighbor list, a distance parameter ε is introduced here. When the distance between two dilated polyhedron elements Δ_{ij} is less than ε, the neighbor pair will be added in the neighbor list. In this study, the parameter ε is proportional to the relative normal velocity of two elements and the computational time step.

The distance between two elements can be determined as

$$\delta_{ij}=\Delta_{ij}\text{-}r_i-r_j \tag{1}$$

where δ_{ij} is the distance between two dilated polyhedrons i and j, Δ_{ij} is the distance between two basic polyhedrons, r_i and r_j are the dilating sphere radii of two elements, respectively. The contacts between dilated polyhedrons will detected exactly from the contact neighbors at each time step.

The contact modes among dilated polyhedron elements can be grouped into four patterns as vertex-edge, edge-edge, vertex-plane, and plane-plane. In the following, we will introduce the numerical algorithm of neighbor search and contact detection of dilated polyhedrons.

For the vertex-edge contact pattern, the essence of contact detection is to determine the shortest distance between the sphere center and the axis of edge cylinder, as shown in Figure 3(b). Similar to Equation (1), we can determine the distance δ between the two elements, i.e, $\delta=|\mathbf{PO}_1|\text{-}r_i-r_j$, here r_i and r_j are the dilating sphere radii of two elements. When $\delta<0$, the two dilated elements are contact in vertex-edge pattern. Here, the vertex-vertex contact pattern is one special case of vertex-edge contact.

For the edge-edge contact pattern, we need to determine the distance between two cylinder axes, which are the two edges of the polyhedrons, as shown in Figure 4. The algorithm of distance calculation of two lines in three dimensions has been developed well. For the vertex-plane contact pattern, we need to calculate the distance between a sphere and a plane, as shown in Figure 5. Firstly, we determine the project of the sphere center O_1 in the plane, and mark as the point P. If the point P is in the plane, we then continue to detect the vertex-plane contact. The distance from the dilating sphere center O_2 to the plane, can be determined easily. Then the distance between the two dilated polyhedrons can be written as $\delta=|\mathbf{PO}_1|\text{-}r_i-r_j$ also. If $\delta<0$, then the vertex-plane contact occurs. For the plane-plane contact pattern, as shown in Figure 6, the distance and contact area of two parallel planes can be determined easily. The edge-plane contact pattern is a special case of the plane-plane contact.

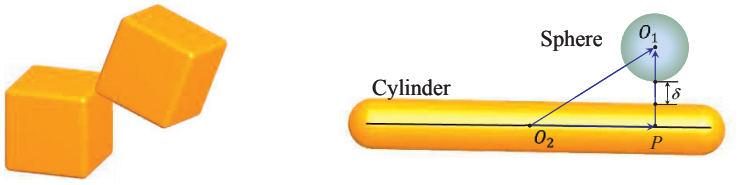

(a) vortex-edge contact (b) contact detection

Figure 3. Contact detection of two dilated polyhedrons in vertex-edge contact

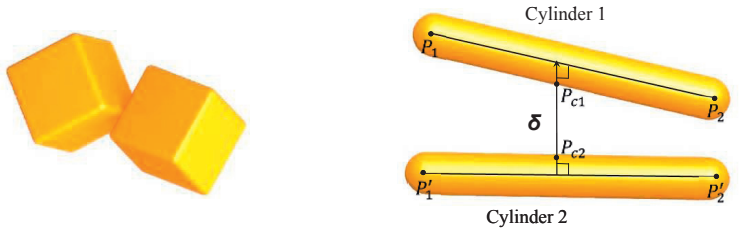

(a) edge-edge contact (b) contact detection

Figure 4. Contact detection of two dilated polyhedrons in edge-edge contact

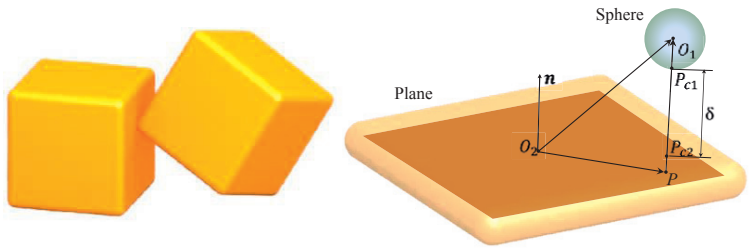

(a) vertect-plane contact (b) contact detection

Figure 5. Contact detection of two dilated polyhedrons in vertex-plane contact

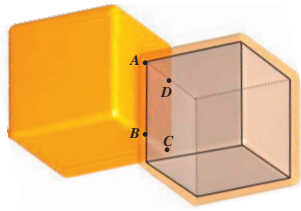

Figure 6. Contact detection of two dilated polyhedrons in plane-plane contact

2.3 Contact force model of dilated polyhedron elements

In the interaction between ballast particles, the nonlinear elastic contact forces are considered in the normal and tangential directions. With the overlap determined in the contact detection, the contact forces are calculated with the contact force model.

For the normal contact force, the nonlinear Hertzian contact model is adopted. This model has been applied widely in the contact simulations of granular materials [12,13]. Here, the contact force in normal direction can be written as

$$\mathbf{F}_{\mathrm{n}} = \frac{2\sqrt{2}G}{3(1-\nu)} R_{\mathrm{e}}^{0.5} \mathbf{x}_{\mathrm{n}}^{1.5} \tag{2}$$

where F_{n} is the normal contact force, G and ν are the shear modulus and Poisson ratio of the ballast materials, R_{e} is the mean radius of the dilating spheres, $\mathbf{x}_{\mathrm{n}}$ is the overlap vector of the two elements.

The tangential contact force is determined with the overlap in tangential direction, which can be obtained incrementally in one time step. At time step m, the tangential force vector is calculated from the tangential force at the previous time step (m-1), and can be written as

$$\mathbf{F}_{\mathrm{t}}^{m} = \mathbf{F}_{\mathrm{t}}^{m-1} - \left[K_{\mathrm{t}} \cdot \Delta t \left(\mathbf{V}_{AB} - \mathbf{V}_{AB} \cdot \mathbf{n} \right) \right] \tag{4}$$

where $\mathbf{F}_{\mathrm{t}}^{m}$ and $\mathbf{F}_{\mathrm{t}}^{m-1}$ are the tangential forces at time steps m and m-1, respectively; K_{t} is the tangential contact stiffness, $\mathbf{V}_{AB}$ is the relative contact force of the two dilating spheres A and B, $\mathbf{n}$ is the unit vector in normal direction, Δt is the time step.

Based on Coulomb friction law, the tangential contact force is limited with the sliding friction, and can be written as

$$\mathbf{F}_{\mathrm{t}}^{\mathrm{m}} = \min\left(\left| \mathbf{F}_{\mathrm{t}}^{\mathrm{m}} \right|, \mu \left| \mathbf{F}_{\mathrm{n}}^{m} \right| \right) \cdot \mathbf{t} \tag{5}$$

where μ is the friction coefficient, $\mathbf{t}$ is the unit vector in tangential direction.

Here, the tangential stiffness is dependent on the normal force, and can be expressed as [13]

$$K_{\mathrm{t}} = \frac{2\left[3G^2 (1-\upsilon) \left| \mathbf{F}_{\mathrm{n}} \right| R_{\mathrm{e}} \right]^{1/3}}{2-\upsilon} \tag{6}$$

The relative velocity of two dilating spheres in contact is written as

$$\mathbf{V}_{AB} = \mathbf{V}_{A} - \mathbf{V}_{B} + \left(\mathbf{r}_{A} \times \boldsymbol{\omega}_{A} \right) - \left(\mathbf{r}_{B} \times \boldsymbol{\omega}_{B} \right) \tag{7}$$

where $\mathbf{r}_{A}$ and $\mathbf{r}_{B}$ are the location vectors from the sphere center the contact point, respectively, $\boldsymbol{\omega}_{A}$ and $\boldsymbol{\omega}_{B}$ are the rotational velocities of spheres A and B, respectively.

In the contact force calculation above, the equations are obtained for the sphere elements. For the contact patterns of edge-edge, and vortex-plane and plane-plane of dilated polyhedrons, the contact force model will be modified considering the contact areas in various contact patterns. Moreover, with the inter-element contact forces, the moments on the dilated polyhedrons can also be determined considering the distance from contact point to the mass center of polyhedrons.

With the contact force and moments obtained at each time step, the velocity and displacement of each dilated polyhedron can be updated. The equations that define translational and rotational motion are standard central difference equations. The matrix that defines the orientation of each element is calculated with quaternion approach.

3. DEM RESUTLS OF BALLAST MATERIALS UNDER CYCLIC LOADINGS

3.1 Setup of the ballast box test in DEM simulation

In this study, the ballast particles are generated with the dilated polyhedrons considering the real size and shapes in engineering application. In the current DEM simulation, the ballast particles are generated following the ballast graduation, as shown in Figure 8. The ballast particles are put into a ballast box randomly, and are packed into static state under the gravity. Then, a sleeper is set on the top of ballast materials. In the construction of ballast particles with dilated polyhedrons, a constant basic sphere radius is adopted as R=0.02m.

For the ballast box, we set the length L=700mn, the width B=300mm. For the sleeper, we set its length L_{s} = 300mm, width B_{s} = 300mm, and mass M_{s} = 34kg. The initial thickness of ballast bed is 365mm here. The initial

packing of ballasts and sleeper location are plotted in Figure 8. The main computational parameters in this DEM simulation are listed in Table 1.

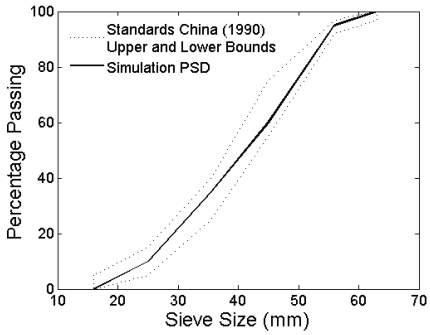

Figure 7. Graduation of ballasts for the DEM simulation

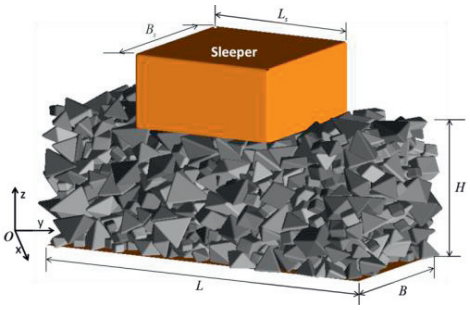

Figure 8. DEM model for railway box experiment

Table 1. Main parameters used in the simulation.

Parameters	Symbols	Values
The density of the particle material	ρ	2600 kg/m^3
Shear modulus	G	20 GPa
Poisson ratio	v	0.3
Coefficient of sliding friction	μ	0.5
Time step	dt	6.48×10^{-6} s
The number of particles	N_p	1034
Initial packing thickness	H	0.38 m
Initial porosity	e_0	0.467
Total mass of railway ballast	M	110 kg

After the initial packing of ballast particles in the ballast box, a cyclic loading is applied on the sleeper top with different frequencies of 3Hz, 6Hz and 10Hz respectively. This cyclic loading is in the range of [3kN, 40kN] with a harmonic function. The sleeper can move in vertical direction under the cyclic loading and the resistance of ballast particles. To model the dynamic behaviors of ballast track on large scale with this ballast box test, the periodic boundaries are adopted in the two horizontal directions of the computational domain.

3.2 Simulation results under cyclic loading with various frequencies

Under the cyclic loadings on the sleeper, the dynamic behaviors of the ballast particles and the sleeper are simulated with DEM. The vertical displacements of the sleeper are obtained with three different frequencies of 3Hz, 6Hz and 10Hz, respectively, as shown in Figure 9. It can be found that the sleeper displacements have a regular fluctuation with the cyclic loading, and increase continuously with increasing cyclic loading time. Under same loading period of 30s, the displacement under high loading frequency is larger than that of low frequency because of the difference of the cyclic number. The more the cyclic number, the larger displacement the sleeper performs. Under high loading frequency f = 10Hz, the displacement curve does not present as smooth as that under low frequency f = 3Hz. For the frequency f = 10Hz, there are two singularity fluctuations at time t = 6.1s and 23.0s, respectively. The significant fluctuations can not be found in the displacement curve of f = 3 Hz. The main reason is rearrangement packing of ballast particles under the cyclic loading. Under the high frequency, the ballasts particles are repacked more easily. The repacking of ballast particles induces the permanent displacement.

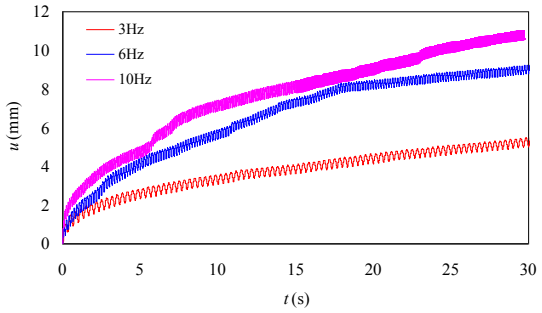

Figure. 9 The sleeper settlement versus time under different frequencies of cyclic loadings

In Figure 10, the cyclic loads and the sleeper displacements are plotted in 3 seconds under the three loading frequencies. We can clearly see that the regular displacement of sleeper under the cyclic load. Both of them have the exact same frequencies. During one period of cyclic loading, the ballast materials have an elastic deformation, which is proportional to the loading magnitude. Meanwhile, the ballast materials also perform a plastic deformation, which is induced by the repacking of ballast particles. The elastic deformation can be recovered when the external force is removed. The plastic deformation will be accumulated with the increase of cyclic number.

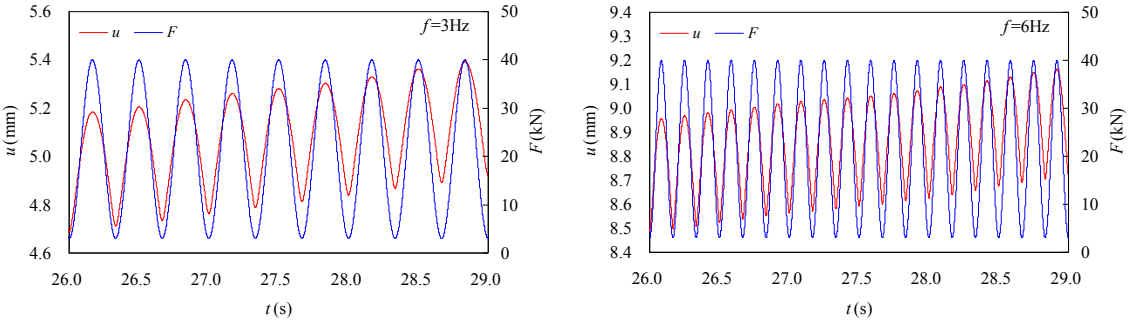

(a) Cyclic loading frequency f = 3Hz

(b) Cyclic loading frequency f = 6Hz

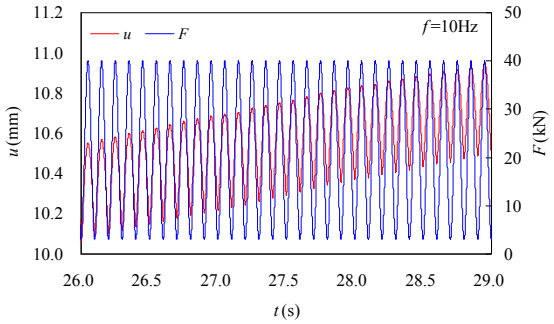

(c) Cyclic loading frequency f = 10Hz

Figure 10. The displacement of sleeper and cyclic loadings versus time.

The curves of the sleepr displacement verus the force are plotted in Figure 11 under different frequencies. In this figure, the curves of the last 0.6mm displacement are zoomed out to display the relationship between displacement

and force more clearly. From the displacement-force curves, we can find the curve density increases with the increase of displacement. This means the sleeper displacement increases under the cyclic loadings, and the slope of the curve becomes more and more steep. The slope of force-displacement can also be defined as the effective stiffness of ballast bed. Moreover, we can also find some special loose zone in the curves. This means the sleeper drops rapidly since the repacking of the ballast particles. This repacking attributes to the permanent displacement of sleeper and the mechanic variation of ballast bed.

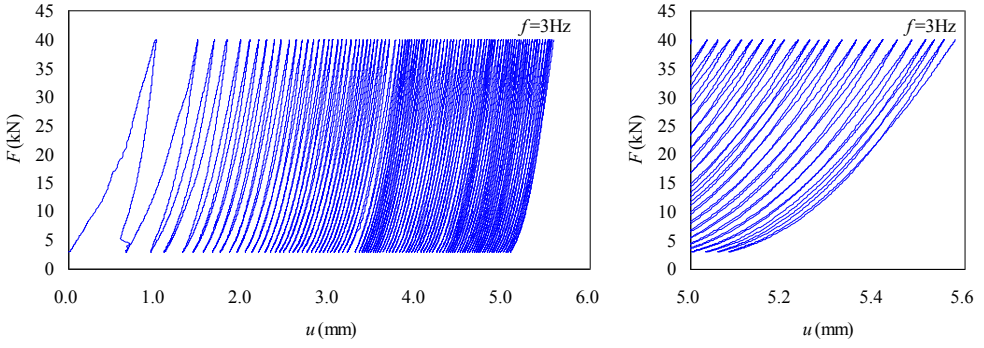

(a) Cyclic loading frequency f = 3Hz

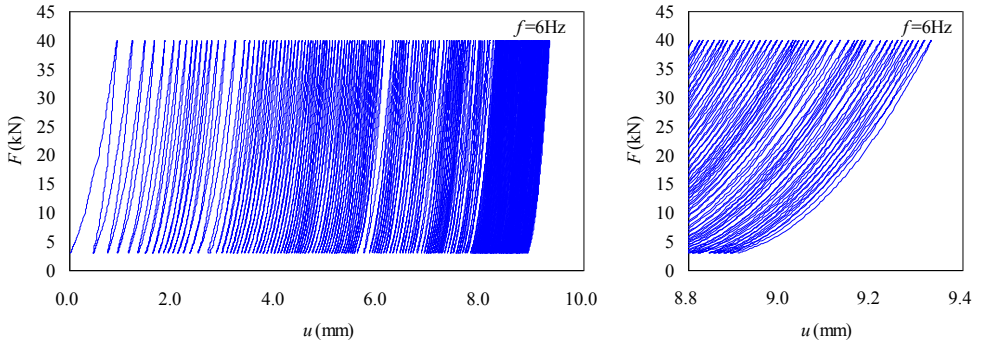

(b) Cyclic loading frequency f = 6Hz

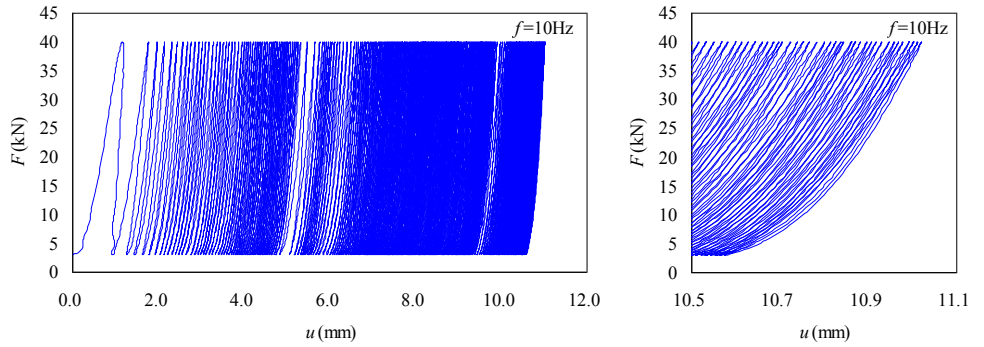

(c) Cyclic loading frequency f = 10Hz

Figure 11. cyclic load as function of displacement of sleeper

The sleeper displacement increases under the cyclic loading. Meanwhile, the mechanic behavior of ballast bed also change with the repacking of ballast particles. One important parameter is the effective stiffness of the ballast bed M_e. Here, we estimate the effective stiffness via the slope the displacement-force curve of the sleeper. At different cyclic loading number under the three loading frequencies, the effective stiffness M_e are plotted in Figure 12 (a). Meanwhile, the accumulated displacement of sleeper at minimum load point of each cyclic loading u is plotted in Figure 12(b). Both of M_e and u increase with cyclic loading number, but the increments decrease gradually. The effective stiffness M_e approaches to different constant under different loading frequencies.

We compare the influences of loading frequency on the effective stiffness and displacement at same cyclic loading number. When the cyclic loading number N =90, the effective stiffness M_e = 75.4, 76.9 and 69.9 kN/mm, the sleeper displacement u = 4.97, 7.04 and 6.62mm, respectively. From the simulated results, we can not find the clear influence of loading frequency on the mechanical behavior of ballast bed. Of course, we should believe the mechanical properties of ballast bed are different under various loading influences. In this present DEM simulation, we only addressed one cases under the three frequencies. The initial packing and repacking patterns of ballast particles also have obvious effects on the dynamic behavior of ballast bed. With more DEM simulations, the statistical data will be applied to investigate the influence of loading frequency.

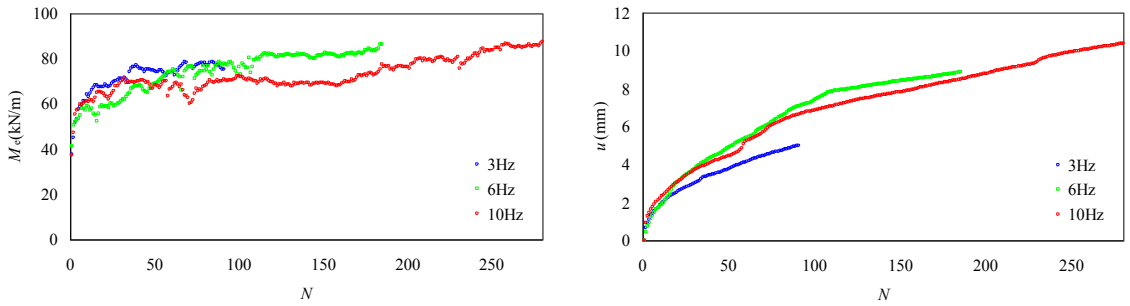

(a) Effective stiffness of ballast bed (b) Permanent displacement of sleeper

Figure 12. The effective stiffness and permanent displacement of the ballast bed under cyclic loadings

4. CONCLUSIONS

To model the irregular shape of railway ballast particle, a dilated polyhedron element is generated with a basic polyhedron and a dilating sphere based on the Minkowski sum approach. The sharpness of the ballast particle is dominated with the dilating sphere radius. The neighbor searching algorithm, contact force model of dilated polyhedron elements are introduced. A ballast box test is constructed with periodic boundary. The ballast particles are generated with this dilated polyhedron method following the standard gradation. The dynamic behaviors of ballast bed are simulated with under cyclic loading with various frequencies. The permanent displacement of the sleeper and the effective stiffness of ballast materials are investigated. Vortex fields of the ballast particles in the ballast box are observed in the DEM simulations. The influences of loading frequencies on the ballast behaviors on macro scale are not significant in this study.

In the future studies, more numerical tests will be performed to analyze statistically the ballast dynamic behaviors. Moreover, the parameter sensitive analysis will be addressed on the settlement and elastic properties of ballast bed considering the ballast shape, size and the loading features. The new dilated polyhedron model with breakage function will be also developed to study the ballast bed behaviors under the influence of crush failure of ballast particles.

ACKNOWLEDGEMENTS

The authors appreciate the discussions on the dilated polyhedral model with Professor Shen Hayley of Clarkson University, USA and Dr. Hopkins Mark A of US Army Cold Regions Research and Engineering Laboratory (CREEL). This study is financially supported by the National Natural Science Foundation of China (41176012, U12342092) and the National Program on Key Basic Research Project (973 Program) (2010CB731502).

REFERENCES

[1] G.R. McDowell, W.L. Lim, A.C Collop, R. Armitage, N.H. Thom, Comparison of ballast index tests for railway trackbeds, Geotechnical Engineering, 157(2004) 151-161.
[2] Lobo-Guerrero S, Vallejo L. Discrete element method analysis of rail track ballast degradation during cyclic loading, Granular Matter, 8(2006) 195-204.
[3] Z. Hossain, B. Indraratna, F. Darve, et al. DEM analysis of angular ballast breakage under cyclic loading, Geomechanics and Geoengineering: An International Journal, 2(2007) 175-181.
[4] H. Huang, E. Tutumluer, Discrete Element Modeling for fouled railroad ballast, Construction and Building Materials, 25(2011) 3306-3312.
[5] W.L. Lim, G.R. McDowell, Discrete element modelling of railway ballast, Granular Matter, 7(2005) 19-29.
[6] Y. Yan, S. Ji, Discrete element modeling of direct shear tests for a granular material, International Journal for Numerical and Analytical Methods in Geomechanics, 34(2010) 978-990.
[7] N.T. Ngo, B. Indraratna, C. Rujikiatkamjorn, DEM simulation of the behaviour of geogrid stabilised ballast fouled with coal, Computers and Geotechnics, 55(2014) 224-231.
[8] M.A. Hopkins, Discrete element modeling with dilated particles, Engineering computations, 21(2003) 422-430.
[9] F. Alonso-Marroquin, Spheropolygons: A new method to simulate conservative and dissipative interactions between 2D complex-shaped rigid bodies, Europhysics Letters, 83(2008) 14001
[10] S.A. Galindo-Torres, D.M. Pedroso, D.J. Williams, H.B. Mühlhaus, Strength of non-spherical particles with anisotropic geometries under triaxial and shearing loading configurations, Granular Matter, 15(2013) 531–542.
[11] S.A. Galindo-Torres, J.D. Muñoz, Minkowski-Voronoi diagrams as a method to generate random packings of spheropolygons for the simulation of soils, Physical Review E, 056713(2010) 1-12.
[12] K.L. Johnson, Contact Mechanics, Cambridge University Press, 1987.
[13] X. Lin, T-T. Ng, A three-dimensional discrete element model using arrays of spheres, Géotechnique, 47(1997) 319-329.